Ring uniformity in amorphous photonic band gap materials

Chih-Ying Yang, Bo-Lin Lai, and Zhi-Hong Xie
Institute of Photonics Technologies, National Tsing Hua University, Hsinchu 30013, Taiwan

Yu-Chueh Hung
Institute of Photonics Technologies, National Tsing Hua University, Hsinchu 30013, Taiwan
and Department of Electrical Engineering, National Tsing Hua University, Hsinchu 30013, Taiwan

(Received 28 June 2021; revised 13 August 2021; accepted 16 August 2021; published 24 August 2021; corrected 27 August 2021)

The existence of photonic band gap (PBG) in amorphous networks has been associated with structural short-range order and internal similarity. In this study we present amorphous networks that possess low degrees of orderness and similarity, yet still exhibit decent PBG forming ability. The robustness of PBG is found to be related to less-deviated ring distributions. We develop regional ring disorder to quantify variations of rings, revealing the complementary roles of regional ring uniformity and local similarity in PBG formation. The evolution of PBG with respect to structural deformation is also presented to elucidate the effect of regional characters on PBG formation. Our study brings new insights towards the understanding of PBG formation in amorphous structures, paving the way for novel design and manipulation of amorphous PBG materials.

DOI: 10.1103/PhysRevB.104.054208

I. INTRODUCTION

Photonic band gap (PBG) materials, which prohibit propagation of electromagnetic modes within a frequency range, have gained considerable attention in the past decades. The generation of PBG is mostly realized by ordered structures, such as photonic crystals [1,2] or liquid crystals [3]. In recent years, amorphous PBG materials also attracted growing interests, motivated by the fascinating structural coloration [4–6] observed in nature. The unusual properties may also find broad applications in sensors [7], random lasers [8,9], optical fibers [10–12], resonators [13], and reconfigurable photonic integrated circuits [14]. There are many existing configurations of amorphous materials that exhibit sizable PBGs, such as randomly packed spheres [15,16], inverse opals [17–19], amorphous gyroid [20] and diamond [21–23] networks, etc. By varying the materials or geometrical parameters, the operation wavelength range and PBG width can be tuned. To fully manipulate the optical properties, however, it is of crucial importance to understand the key structural characters that govern the formation of PBGs. The resolution is particularly challenging for three-dimensional (3D) amorphous structures, given the variety and complexity of topology and spatial organization.

Research efforts have been devoted to examining the correlation between structural characters and PBG properties of amorphous materials. To inspect the structural features, several fundamental characterizations, such as Fourier power spectra [24,25], structure factor [26,27], radial distribution function [28], and structural order parameter [29], are carried out to yield information related to spatial distribution and local topology. From the analysis of these measures, it is revealed that the existence of PBG is closely associated with structural short-range order [30–32]. PBG forming ability is also found to be closely related to local self-uniformity (LSU) as proposed by Sellers *et al.* [20]. They showed that amorphous networks assembled with highly similar local units, manifested by significant LSU, are beneficial to PBG formation. However, in review of these studies, the amorphous structures are normally generated by prescribed optimization protocols [20,33]. With the constraints imposed in the algorithms, the resulting topology tends to evolve toward a more uniform spatial distribution. The finite degree of structural deformation somewhat confines the topological scenarios that can be explored.

In this study we present representative amorphous networks that possess low degrees of short-range order and local similarity as indicated by the measures, yet still exhibit decent PBG forming ability. Rod-connected amorphous networks with trivalent vertices and a refractive index of 3.6 are used as model systems. We introduce additional structural deformation on annealed amorphous networks and find that the resulting structure's PBG is quite robust against distortion of local units. It indicates that the scope of structural measures of PBG materials needs to be broadened beyond local comparison. In fact, in amorphous solids, medium-range order, evaluated by ring analysis, has been discussed as a character [34–37], which extends the structural analysis toward a more regional aspect. The previous measures of PBG materials have been primarily related to short-range order, while the contribution of longer-scale structural feature to PBG formation remains unclear. We explore the effect of ring characteristics on PBG properties and show that ring uniformity has a great impact on the formation of PBG in amorphous networks. In addition, the PBG forming ability is associated with the interplay between local similarity and ring uniformity. The PBG forming ability with respect to different structural characters will also be discussed.

II. PBG FOR AMORPHOUS NETWORKS

We start our discussion by presenting two rod-connected amorphous structures with a similar PBG forming ability. The dielectric fill fraction of the network is set to be 20%, which is around the level for such rod-connected networks to show optimized PBG [20,38]. The first structure is a continuous random network (CRN), where a 216-vertex network is constructed by the modified Wooten-Winer-Weaire (WWW) algorithm [20,39,40]. The details of the algorithm are described in the Supplemental Material [41]. Figure 1(a) shows a representative CRN structure. Via the WWW algorithm, an amorphous trivalent network tends to evolve toward an ideal gyroid. We examine the geometrical characteristics of the CRN, presented by edge lengths d, interedge angles θ, dihedral angles ϕ, and skew angles χ, as shown in Figs. 1(b) and 1(c). The distribution of d exhibits a finite width centered around d_0, where d_0 is the edge length of the skeletal gyroid network. The distributions of θ, ϕ, and χ are centered at 120°, 70.5°/105.5°, and 90°, respectively, resembling those of an ideal gyroid network. The radial distribution function (RDF) is calculated to reveal the spatial correlation of vertices [28]. Figure 1(d) shows the RDF of the CRN structure, which displays evident peaks, indicating well-distributed vertices in space possessing short-range order. The Fourier transform of the network shown in the inset figure displays concentric spherical shells without discrete Bragg peaks, indicating structural isotropy without long-range order. The band structure of the CRN is calculated by the finite-difference time-domain method (FDTD, Lumerical Inc.) as shown in Fig. 1(e). The simulation settings are described in the Supplemental Material [42]. A complete PBG is observed in the frequency range of 0.216 to 0.231 (a/λ). The band gap width $\Delta\omega/\omega_0$, defined as the ratio of band gap size $\Delta\omega$ to middle frequency ω_0, is around 6.8%.

The second structure, denoted as CRN′-RV, is a CRN undergoing relocation of vertex (RV) algorithm, where vertices of the network are randomly positioned within some finite relocation distances. The prime of CRN′-RV is meant to show that CRN′-RV is derived from a CRN of better annealing conditions with respect to the CRN in Fig. 1(a). Due to better annealing conditions, the CRN′ before vertex relocation yields a band gap width of 17.4%. The details of the RV algorithm are described in the Supplemental Material [43]. CRN′-RV is shown in Fig. 1(f), displaying a more disordered appearance than CRN. The same analyses for CRN′-RV structures are presented in Figs. 1(g) and 1(h). The edge lengths and interedge angles are distributed around centered values, whereas dihedral angles and skew angles are dispersed. The RDF and the Fourier transform of the network are shown in Fig. 1(i). The Fourier pattern exhibits a similar concentric shape, indicating isotropic structural property. However, the RDF displays an evenly distributed statistic without featured peaks in the profile. Compared to CRN, we can see that CRN′-RV possesses a relatively low degree of short-range order as indicated by the geometrical properties. The band structure of CRN′-RV is shown in Fig. 1(j). A complete PBG for CRN′-RV is allocated in the frequency range from 0.218 to 0.231 (a/λ). Despite distinct geometrical features for CRN and CRN′-RV, both structures exhibit surprisingly similar PBG properties.

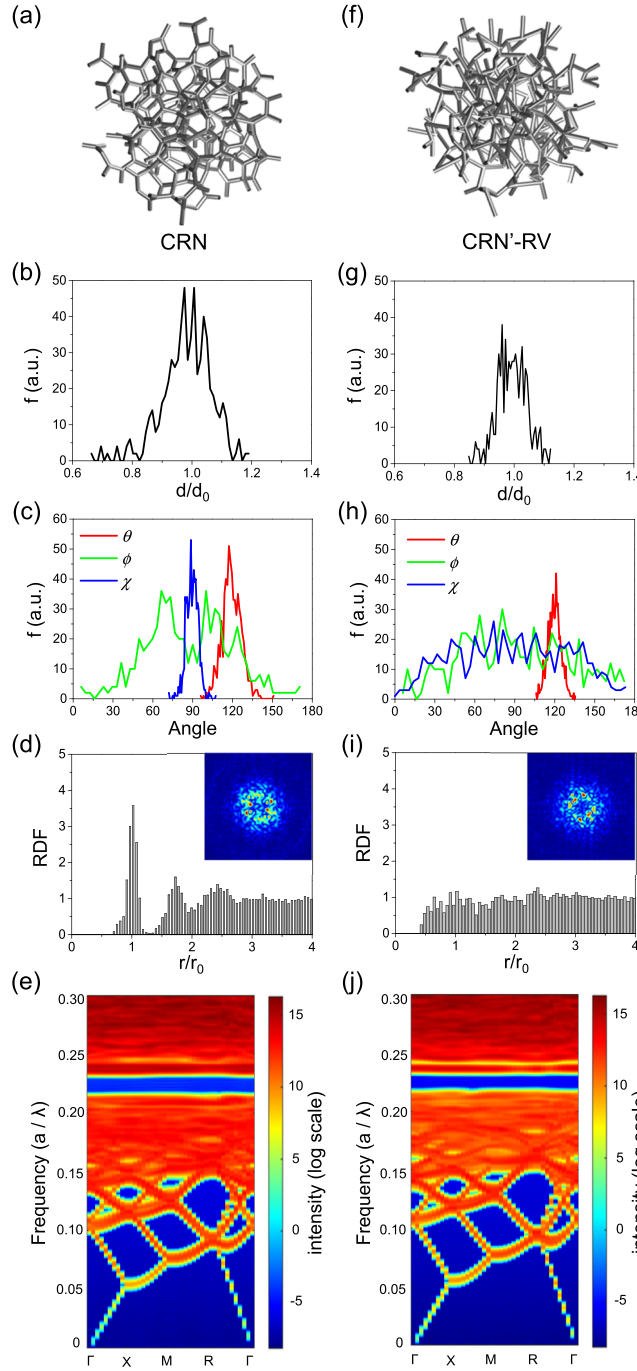

FIG. 1. Amorphous network morphologies of CRN (a) and CRN′-RV (f) with a similar PBG width. The edge length d, interedge angle θ, dihedral angle ϕ, skew angles χ, radial distribution function (RDF), and band structures for CRN and CRN′-RV are plotted in (b)–(e) and (g)–(j), respectively. The Fourier transform analyses of networks are shown as the insets of RDF distributions.

III. LOCAL SIMILARITY AND PBG

Among the present structural analyses for amorphous networks, it has been found that similarity of local element is strongly associated with the formation ability of PBG. One qualitative evaluation is LSU (Φ_{22}), calculated by the mean of similarity measuring function ϕ_{nl}, where ϕ_{nl} describes the

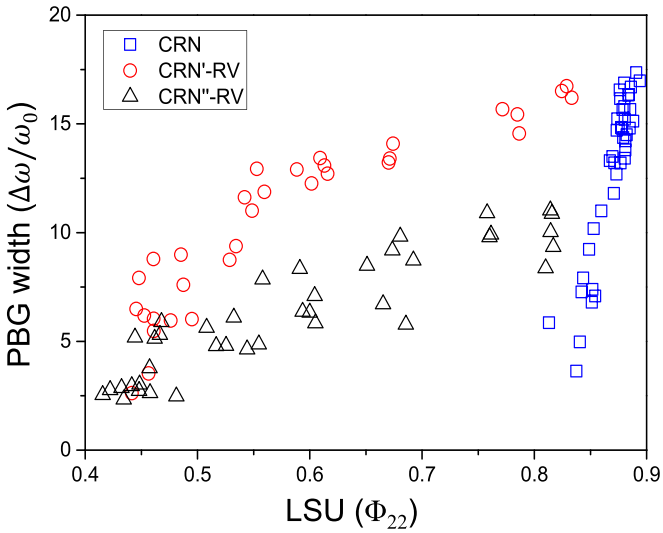

FIG. 2. Photonic band gap (PBG) width ($\Delta\omega/\omega_0$) versus local self-uniformity (LSU) (Φ_{22}) of CRN (blue squares), CRN′-RV (red circles), and CRN″-RV (black triangles).

similarities for all pairs of trees with depth n and locality l (see definitions in the Supplemental Material [44]). It was found that amorphous networks with a high level of LSU ($\Phi_{22} > 0.7$) is favorable for PBG formation [20]. We carry out the LSU (Φ_{22}) analysis for the two structures in Fig. 1 to examine their local similarity. Our calculation shows that Φ_{22} of the CRN structure is 0.82, whereas Φ_{22} of the CRN′-RV structure is 0.48. It indicates that CRN′-RV possesses a low level of local similarity and its LSU is also far below the satisfactory margin for PBG occurrence. From the geometrical features in Figs. 1(g)–1(i) and LSU analysis, the structural characters of CRN′-RV exhibit diverse distributions of dihedral and skew angles, featureless RDF, as well as a low level of local similarity. Yet, the PBG forming ability is comparable with the structures displaying more evident features of short-range order and high local similarity. It implies that PBG formation in CRN′-RV is attributed to some geometrical characteristics not revealed by present structural measures.

For a more comprehensive analysis, we construct sets of amorphous networks undergoing vertex relocation to examine how LSU and PBG width are correlated. We present the analysis for CRN structures undergoing vertex relocation derived from two different initial CRNs, denoted as CRN′-RV and CRN″-RV, where CRN′ is better annealed than CRN″. We gradually increase the vertex relocation distance and examine the corresponding Φ_{22} and PBG widths. In Fig. 2 the PBG widths ($\Delta\omega/\omega_0$) versus LSU are plotted for CRN′-RV and CRN″-RV by circles and triangles, respectively. CRNs with different annealing levels are also plotted by squares for comparison. In all the structures, the Φ_{22} values are positively correlated with PBG widths, but the distributions display a rather different behavior. For CRNs, LSU mostly falls in the range of 0.8–0.9, implying that only CRNs possessing significant local similarity exhibit sizable PBG. In addition, the gap width narrows down rapidly with decreased Φ_{22}. For CRN′-RV and CRN″-RV (referred to as RV series hereafter), the values of LSU for sizable PBG distribute within a broad span. As opposed to the steep PBG decline in CRN, PBG of the RV series decreases in a more progressive manner. For example, PBG widths of CRN′-RV just decrease by 3% in spite of an apparent reduction of Φ_{22} from 0.84 to 0.65. The behavior of the RV series distinctly diverges from the intrinsic CRN structural character. It is attributed to the application of vertex relocation, which introduces the other degree of structural deformation. To further examine the effect of vertex relocation on PBG properties, we also apply the RV algorithm on an ordered gyroid network, referred to as Gyroid-RV. The LSU distribution is calculated while increasing the vertex relocation distance, and the corresponding gap width is plotted as shown by diamond dots in Fig. S5 in the Supplemental Material [45]. Before vertex relocation, the gyroid network has a gap width of 24% and a unity Φ_{22}. As the range of vertex location is extended, Φ_{22} and PBG width decrease simultaneously and the trend follows a similar behavior as the RV series. It suggests that vertex relocation has a similar impact on PBG properties for both ordered and disordered structures.

IV. FROM LOCAL TO REGIONAL ANALYSIS

To elucidate the geometrical variations due to different structure construction algorithms, we look into the geometrical variations resulting from different construction algorithms. For simplicity, two networks with connected trihedral in Fig. 3(a) are illustrated to outline the features of structure construction. We first depict the structure undergoing modified WWW algorithm for CRN construction as shown in the upper panel. The evolution of CRN involves the introduction of Stone-Wale defects and topological relaxation in order to reduce Keating potential energy of geometrical constraints [20,40]. Afterwards, edges $\overline{AF}$ and $\overline{BC}$ are reconnected to be $\overline{AC}$ and $\overline{BF}$ due to bond transposition and vertices are relaxed to optimized locations. The algorithm forces CRN to evolve toward ideal gyroidal topology, giving rise to more uniform geometrical features. In the lower panel, we depict the construction of CRN′-RV with an initial structure CRN′. After applying the RV algorithm, all vertices are randomly relocated within a finite distance. The connectivity of edges remains the same, yet the trihedral units experience a dramatic deformation. The uncorrelated perturbation in turn has a great impact on the dihedral angles and skew angles, in line with the broad angle distributions in Fig. 1(h). The dramatic disruption of local units also leads to the wide distribution of Φ_{22}, ranging from 0.4 to 1 as shown in Fig. 2. In addition, it is noticed that PBGs of the RV series are more robust against low Φ_{22}, indicating the optical properties are less sensitive with respect to variations of local units.

To further examine how geometrical features are correlated with LSU, we illustrate a two-dimensional (2D) network in Fig. 3(b) to exemplify the procedures. The network can be decomposed into trees A, B, and C. The center of each tree is marked in yellow. Vertices with depths 1 and 2 from the center vertex are marked in green and blue, respectively. In evaluating LSU, trees are maximally aligned through permutation and rotation to examine the level of similarity. We illustrate the comparison by depicting the overlap of trees when they are maximally aligned by root edges. For a scenario where

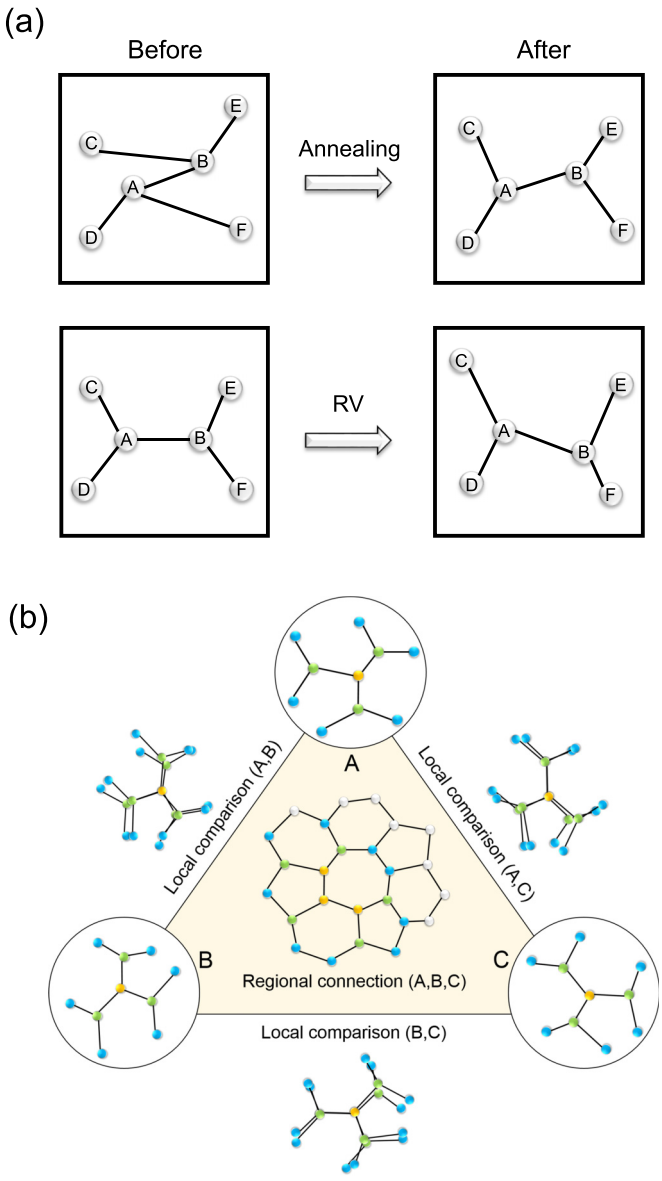

FIG. 3. (a) Illustrations of the constructive process of CRN (upper panel) and CRN′-RV (lower panel). (b) An illustration shows the comparison of local units (trees). Comparison of local units is carried out by rotation and permutation of trees in order to optimize the alignment. The center of each tree is marked in yellow. Vertices with depths 1 and 2 from the center vertex are marked in green and blue, respectively.

the trees are geometrically similar, the comparison results in a high level of local similarity. However, the comparison is carried out after permutation and rotation of trees. The relative organization of the trees in a 3D space is not taken into consideration in the LSU evaluation. On the other hand, vertex relocation yields a scenario where network connectivity of local units is fully preserved and the relative organization of local units remains unchanged. Without bond transposition, the spatial regions in the air fraction may be just slightly disturbed in spite of a pronounced deformation of local units. It further implies that the robustness of PBG may be associated with the geometrical character of adjacent spatial regions

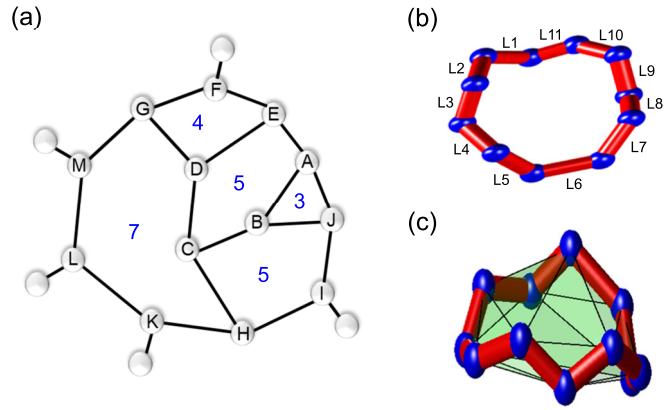

FIG. 4. (a) A simplified 2D network is illustrated for ring analysis. Five SP rings with the ring number denoted can be identified in the network based on the SP criterion. Ring analysis is carried out by comparing the chosen ring with its neighboring rings. A ring of the CRN is depicted to demonstrate the ring length (b) and ring volume (c). Edges and vertices of the ring are marked in red and blue, respectively. The ring length is the summation of edge length from L1 to L11. The ring volume is calculated by convex hull of the ring, which is enclosed by the green trisurfaces.

inherited from the initial CRNs. Such structural feature is closely related to multiple connected local units in close proximity. That is, the corresponding structural analysis needs to be spatially extended toward a more regional extent beyond local units.

V. RING INHOMOGENEITY AND REGIONAL RING DISORDER

To evaluate regional contributions, we carry out structural analysis based on rings of a network. Ring statistics have been utilized to characterize structural properties in amorphous materials, where the medium-range order has been discussed in glass and amorphous solids [34,37]. Since the span of rings extends spatially beyond local multihedral units, ring analysis reveals information in a more regional and medium-range extent [46,47]. In the definition, a ring comprises a closed loop connected by vertices and edges, and is uniquely defined based on the shortest-path (SP) criterion [48]. An α ring is referred to a ring satisfying the SP criterion with a vertex number α. We propose a general model of ring inhomogeneity (RI), contributed from the variation of rings by comparing the geometrical features. RI_n is the RI of the nth ring, and is mathematically expressed as

$$\mathrm{RI}_n = \frac{1}{P_n}\sum_{k=1}^{P_n}\frac{|\,\chi_{nk}-\chi_n\,|}{\chi_n}, \tag{1}$$

where χ_n and χ_{nk} are the geometrical features of the chosen nth ring and the neighboring kth ring sharing at least one edge, respectively. The total number of neighboring rings of the nth ring is P_n. A 2D network is illustrated in Fig. 4(a) as a simplified example for ring analysis. This network consists of multiple rings with vertex numbers of 3, 4, 5, and 7. Assuming that a ring A-B-C-D-E is chosen for evaluation, there are four

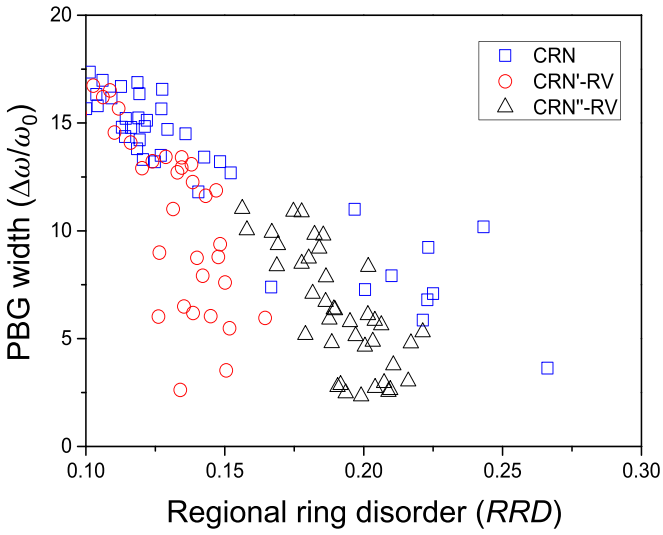

FIG. 5. Regional ring disorder (RRD) of amorphous networks versus PBG width. CRN, CRN′-RV, and CRN″-RV are marked in blue squares, red circles, and black triangles, respectively.

rings connected to the chosen ring, which are rings A-B-J, D-E-F-G, B-C-H-I-J, and C-H-K-L-M-G-D. The corresponding geometrical features of chosen and connected rings are compared to perform evaluation of RI. The level of RI is associated with the nonuniform characteristics of geometrical features between the chosen ring and the neighboring rings. We can see a ring generally comprises connected vertices across a few trihedral units. As a result, ring-based analysis reveals spatial information beyond comparison of local trees as described previously in Fig. 3(b), yielding geometrical characteristics towards more regional aspect. To quantify the regional effect contributed from ring variations, we develop an index as regional ring disorder (RRD) by

$$\mathrm{RRD} = \frac{\sum_{n=1}^{N}(\mathrm{RI}_n)}{N}, \tag{2}$$

where RI_n is the ring inhomogeneity of the nth ring, and N is the total number of rings of the network. In our analysis we have conducted comprehensive studies based on different ring parameters. We found there are two predominant geometrical features that are most relevant to manifest the regional characters affecting PBG. One is the variation of ring lengths. Ring length is the summation of edge lengths of a ring as depicted in Fig. 4(b), which is relevant to the length scale that a ring extends. The other is related to the stereoscopic feature of the ring as calculated by the ring volume. Ring volume is referred to the volume of convex hull [49] bounded by vertices of a ring, as depicted in Fig. 4(c). The convex hull entangles stereoscopic features of a ring as a rational volume, relevant to the 3D spatial occupation of a ring.

We calculate RRD contributed from ring length and ring volume by the process flow as shown in Fig. S6 [50]. RRD of the three networks and the corresponding PBG widths are shown in Fig. 5. We can see that RRD is negatively correlated with PBG width for all the networks, indicating that the variation of rings is closely related to PBG forming ability. We can further examine how RRD varies when structures undergo different deformations. For CRN, RRD ranges from 0.1 to 0.28 depending on the annealing level. A better annealed CRN displays a lower level of RRD. For the RV series, CRN′-RV is derived from a better annealed network, so RRD values are smaller compared to those of CRN″-RV. From the analysis, we can see a relatively large variation of RRD is displayed for CRNs of different annealing levels. It is ascribed to bond transposition in the annealing process, which leads to a larger ring variation. On the other hand, vertex relocation only involves shifts of vertices without varying the network connectivity. For better annealed networks, the disruption on ring statistics owing to vertex shift is less severe. This can be revealed by a smaller RRD variation (0.1–0.17) in CRN′-RV. The RRD disruption is even less pronounced for an ordered gyroid undergoing vertex relocation. For example, the change of RRD of an ordered gyroid undergoing vertex relocation is only around 0.03 with a relatively large relocation distance of 2.5 as shown in Fig. S7 [51].

We further compare the three networks by their RRD and LSU analyses. For CRN, the annealing process results in networks with high Φ_{22} within a finite range (0.8–0.9), yet a wide distribution of RRD. For the RV series, vertex relocation leads to networks of widely distributed LSU and smaller RRD. It shows the distinct structural characteristics introduced by annealing and vertex shift. In addition, to yield sizable PBG, networks of low Φ_{22} also possess low level of RRD. That is, networks with less similar local units exhibit a more uniform property in ring statistics. It indicates local similarity and ring uniformity play seemingly complementary roles in the formation of PBG.

VI. ROBUSTNESS OF PBG

PBG formation in 3D dielectric networks has been associated with Bragg and Mie scattering [20,27,52]. The optical characteristics are normally manifested by the localized distributions of electromagnetic fields around the gap edge, where the localization properties can be characterized by the inverse participation ratio [53,54]. We monitor the modes with a high inverse participation ratio around the band edges, referred to as the band-edge states, to examine the localized properties. Specifically, the fields of lower band-edge states are well localized in the dielectric regions, whereas those of higher band-edge states are localized in the air fraction. To feature the properties of localized states, we examine the field distributions of the CRN structure at the lower and higher band edges as shown in Figs. 6(a) and 6(b), respectively. It is observed that the dielectric band below the PBG is strongly localized in the small dielectric ring, whereas the air band at the upper edge is localized at a space surrounded by a larger ring. It implies the present localized fields are more spatially confined by a 3D space, enclosed by closed loop rings.

As featured by the geometrical dependence of localized fields, geometries of dielectric local units may be more critical in governing the lower band-edge modes, while geometrical features of the 3D air regions play a more dominant role for the higher band-edge modes. When the network is deformed, PBG is disturbed in a way that reflects the corresponding structural characters. Similar observation is also reported in 2D photonic foam, where the upper frequency of PBG is most

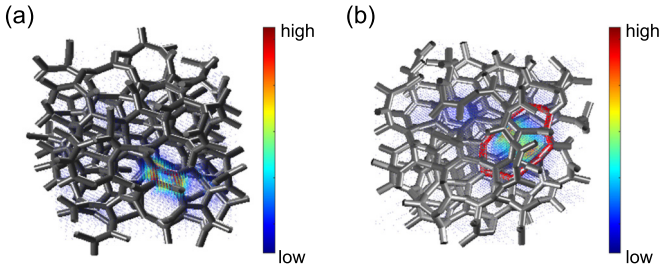

FIG. 6. Localized modes of CRN at the lower band edge (a) and higher band edge (b). The specific rings surrounding the localized modes are marked in red.

related to the diversity of dielectric nodes coordination (valences) [55]. Diverse node distribution may split the air space into a less-uniform group, leading to reduction of PBG width. As described in the previous section, when vertices undergo a moderate shift, the air fractions of the network are less disturbed in spite of the deformation of dielectric local units. The RV algorithm yields a scenario where spatial regions in the air fractions are better preserved, leading to less disturbance of the higher band-edge states. An example is depicted in Fig. S8 to show how PBG evolves with respect to relocation distance for CRN′-RV [56]. As the relocation distance increases, a narrowing PBG is observed, yet with different behaviors in the lower and higher band edges. With a moderate relocation distance varying from 0 to 1.5, the lower band-edge frequency exhibits a pronounced shift, whereas the movement of higher band-edge frequency is less apparent. It is ascribed to a larger distortion of dielectric local units under vertex relocation, resulting in more severe disruption to localized resonances within the dielectric. On the other hand, the 3D spatial air regions are relatively less disturbed under vertex relocation. The resonances for higher band-edge states are less disrupted, manifested by the subtle higher band-edge frequency shift. While further increasing the relocation distance above 2, the distortion in the air regions is also significant. The shift of the higher band edge then becomes comparable to that of the lower band edge toward PBG narrowing.

VII. CONCLUSION

In this work we carry out structural and photonic band gap analysis for continuous random networks undergoing geometrical variations. By virtue of the wide degree of structural variations via bond transposition and vertex relocation, we present amorphous networks that exhibit decent band gap forming ability in spite of low degrees of short-range order and local similarity. It reveals that the band gap forming ability is ascribed to structural features beyond similarity of local units. We develop geometrical analysis based on rings to qualitatively evaluate regional characters, and show the robustness of PBG against low local similarities is attributed to the maintenance of ring uniformity. The regional attribute can be further manifested by the spatial distribution of localized fields at the band edges, where the evolution of band gap can also be observed in reflection of the corresponding structural distortion. The methodology can be applied to a wide variety of disordered networks, advancing the comprehension of amorphous PBG materials.

ACKNOWLEDGMENTS

We thank R. M. Ho, Y. W. Chiang, and C. C. Chen for valuable comments and discussion. This work is supported by the Ministry of Science and Technology (MOST) in Taiwan under Grants No. 108-2221-E-007-101-MY2, No. 109-2224-E-110-002-, and No. 110-2628-E-007-006-.

[1] C. López, Materials aspects of photonic crystals, Adv. Mater. **15**, 1679 (2003).

[2] A. Blanco, E. Chomski, S. Grabtchak, M. Ibisate, S. John, S. W. Leonard, C. Lopez, F. Meseguer, H. Miguez, J. P. Mondia, G. A. Ozin, O. Toader, and H. M. van Driel, Large-scale synthesis of a silicon photonic crystal with a complete three-dimensional bandgap near 1.5 micrometres, Nature (London) **405**, 437 (2000).

[3] J. Hwang, M. H. Song, B. Park, S. Nishimura, T. Toyooka, J. W. Wu, Y. Takanishi, K. Ishikawa, and H. Takezoe, Electro-tunable optical diode based on photonic bandgap liquid-crystal heterojunctions, Nat. Mater. **4**, 383 (2005).

[4] M. Iwata, M. Teshima, T. Seki, S. Yoshioka, and Y. Takeoka, Bio-inspired bright structurally colored colloidal amorphous array enhanced by controlling thickness and black background, Adv. Mater. **29**, 1605050 (2017).

[5] P. Liu, J. Chen, Z. Zhang, Z. Xie, X. Du, and Z. Gu, Bio-inspired robust non-iridescent structural color with self-adhesive amorphous colloidal particle arrays, Nanoscale **10**, 3673 (2018).

[6] B. Q. Dong, X. H. Liu, T. R. Zhan, L. P. Jiang, H. W. Yin, F. Liu, and J. Zi, Structural coloration and photonic pseudogap in natural random close-packing photonic structures, Opt. Express **18**, 14430 (2010).

[7] I. El-Kady, M. Reda Taha, and M. Su, Application of photonic crystals in submicron damage detection and quantification, Appl. Phys. Lett. **88**, 253109 (2006).

[8] H. Cao, Y. G. Zhao, S. T. Ho, E. W. Seelig, Q. H. Wang, and R. P. H. Chang, Random Laser Action in Semiconductor Powder, Phys. Rev. Lett. **82**, 2278 (1999).

[9] J. Liu, P. Garcia, S. Ek, N. Gregersen, T. Suhr, M. Schubert, J. Mørk, S. Stobbe, and P. Lodahl, Random nanolasing in the Anderson localized regime, Nat. Nanotechnol. **9**, 285 (2014).

[10] B. Abaie, M. Peysokhan, J. Zhao, J. E. Antonio-Lopez, R. Amezcua-Correa, A. Schülzgen, and A. Mafi, Disorder-induced high-quality wavefront in an Anderson localizing optical fiber, Optica **5**, 984 (2018).

[11] B. Abaie, E. Mobini, S. Karbasi, T. Hawkins, J. Ballato, and A. Mafi, Random lasing in an Anderson localizing optical fiber, Light: Sci. Appl. **6**, e17041 (2017).

[12] G. Ruocco, B. Abaie, W. Schirmacher, A. Mafi, and M. Leonetti, Disorder-induced single-mode transmission, Nat. Commun. **8**, 14571 (2017).

[13] S. Li, Z.-J. Wang, L.-S. Chen, X. Sun, and T. F. George, Collective behavior and disorder-induced resonator of random lasers, Appl. Phys. Lett. **86**, 171109 (2005).

[14] M. A. Mohammed, J. Melskens, R. Stabile, F. Pagliano, C. Li, W. M. Kessels, and O. Raz, Metastable refractive index manipulation in hydrogenated amorphous silicon for reconfigurable photonics, Adv. Opt. Mater. **8**, 1901680 (2020).

[15] A.-P. Hynninen, J. H. Thijssen, E. C. Vermolen, M. Dijkstra, and A. Van Blaaderen, Self-assembly route for photonic crystals with a bandgap in the visible region, Nat. Mater. **6**, 202 (2007).

[16] S. Torquato, T. M. Truskett, and P. G. Debenedetti, Is Random Close Packing of Spheres Well Defined?, Phys. Rev. Lett. **84**, 2064 (2000).

[17] Z.-Y. Li and Z.-Q. Zhang, Fragility of photonic band gaps in inverse-opal photonic crystals, Phys. Rev. B **62**, 1516 (2000).

[18] C. I. Aguirre, E. Reguera, and A. Stein, Tunable colors in opals and inverse opal photonic crystals, Adv. Funct. Mater. **20**, 2565 (2010).

[19] R. C. Schroden, M. Al-Daous, C. F. Blanford, and A. Stein, Optical properties of inverse opal photonic crystals, Chem. Mater. **14**, 3305 (2002).

[20] S. R. Sellers, W. Man, S. Sahba, and M. Florescu, Local self-uniformity in photonic networks, Nat. Commun. **8**, 14439 (2017).

[21] K. Edagawa, S. Kanoko, and M. Notomi, Photonic Amorphous Diamond Structure with a 3D Photonic Band Gap, Phys. Rev. Lett. **100**, 013901 (2008).

[22] B. R. Djordjević, M. F. Thorpe, and F. Wooten, Computer model of tetrahedral amorphous diamond, Phys. Rev. B **52**, 5685 (1995).

[23] H. Yin, B. Dong, X. Liu, T. Zhan, L. Shi, J. Zi, and E. Yablonovitch, Amorphous diamond-structured photonic crystal in the feather barbs of the scarlet macaw, Proc. Natl. Acad. Sci. USA **109**, 10798 (2012).

[24] L. Shi, H. Yin, R. Zhang, X. Liu, J. Zi, and D. Zhao, Macroporous oxide structures with short-range order and bright structural coloration: A replication from parrot feather barbs, J. Mater. Chem. **20**, 90 (2010).

[25] K. Ueno, A. Inaba, Y. Sano, M. Kondoh, and M. Watanabe, A soft glassy colloidal array in ionic liquid, which exhibits homogeneous, non-brilliant and angle-independent structural colours, Chem. Commun. **2009**, 3603 (2009).

[26] S. Torquato and F. H. Stillinger, Local density fluctuations, hyperuniformity, and order metrics, Phys. Rev. E **68**, 041113 (2003).

[27] M. Florescu, S. Torquato, and P. J. Steinhardt, Designer disordered materials with large, complete photonic band gaps, Proc. Natl. Acad. Sci. USA **106**, 20658 (2009).

[28] L. Shi, Y. Zhang, B. Dong, T. Zhan, X. Liu, and J. Zi, Amorphous photonic crystals with only short-range order, Adv. Mater. **25**, 5314 (2013).

[29] S. F. Liew, J.-K. Yang, H. Noh, C. F. Schreck, E. R. Dufresne, C. S. O'Hern, and H. Cao, Photonic band gaps in three-dimensional network structures with short-range order, Phys. Rev. A **84**, 063818 (2011).

[30] S. Torquato, G. Zhang, and F. H. Stillinger, Ensemble Theory for Stealthy Hyperuniform Disordered Ground States, Phys. Rev. X **5**, 021020 (2015).

[31] L. S. Froufe-Pérez, M. Engel, P. F. Damasceno, N. Muller, J. Haberko, S. C. Glotzer, and F. Scheffold, Role of Short-Range Order and Hyperuniformity in the Formation of Band Gaps in Disordered Photonic Materials, Phys. Rev. Lett. **117**, 053902 (2016).

[32] L. S. Froufe-Pérez, M. Engel, J. J. Sáenz, and F. Scheffold, Band gap formation and anderson localization in disordered photonic materials with structural correlations, Proc. Natl. Acad. Sci. USA **114**, 9570 (2017).

[33] M. J. Cliffe, A. P. Bartók, R. N. Kerber, C. P. Grey, G. Csányi, and A. L. Goodwin, Structural simplicity as a restraint on the structure of amorphous silicon, Phys. Rev. B **95**, 224108 (2017).

[34] S. R. Elliott, Medium-range structural order in covalent amorphous solids, Nature (London) **354**, 445 (1991).

[35] S. Le Roux and P. Jund, Ring statistics analysis of topological networks: New approach and application to amorphous GeS_2 and SiO_2 systems, Comput. Mater. Sci. **49**, 70 (2010).

[36] Y. Hiraoka, T. Nakamura, A. Hirata, E. G. Escolar, K. Matsue, and Y. Nishiura, Hierarchical structures of amorphous solids characterized by persistent homology, Proc. Natl. Acad. Sci. USA **113**, 7035 (2016).

[37] S. S. Sørensen, C. A. Biscio, M. Bauchy, L. Fajstrup, and M. M. Smedskjaer, Revealing hidden medium-range order in amorphous materials using topological data analysis, Sci. Adv. **6**, eabc2320 (2020).

[38] M. Maldovan and E. L. Thomas, Diamond-structured photonic crystals, Nat. Mater. **3**, 593 (2004).

[39] F. Wooten, K. Winer, and D. Weaire, Computer Generation of Structural Models of Amorphous Si and Ge, Phys. Rev. Lett. **54**, 1392 (1985).

[40] G. T. Barkema and N. Mousseau, High-quality continuous random networks, Phys. Rev. B **62**, 4985 (2000).

[41] See Supplemental Material at http://link.aps.org/supplemental/10.1103/PhysRevB.104.054208 for details of the modified Wooten-Winer-Weaire algorithm.

[42] See Supplemental Material at http://link.aps.org/supplemental/10.1103/PhysRevB.104.054208 for details of the simulation settings of band structure calculations.

[43] See Supplemental Material at http://link.aps.org/supplemental/10.1103/PhysRevB.104.054208 for details of the algorithm of random relocation of vertices.

[44] See Supplemental Material at http://link.aps.org/supplemental/10.1103/PhysRevB.104.054208 for details of calculations of LSU.

[45] See Supplemental Material at http://link.aps.org/supplemental/10.1103/PhysRevB.104.054208 for PBG width vs LSU of an ordered gyroid under vertex relocation.

[46] A. Pandey, P. Biswas, B. Bhattarai, and D. A. Drabold, Realistic inversion of diffraction data for an amorphous solid: The case of amorphous silicon, Phys. Rev. B **94**, 235208 (2016).

[47] V. L. Deringer and G. Csányi, Machine learning based interatomic potential for amorphous carbon, Phys. Rev. B **95**, 094203 (2017).

[48] D. S. Franzblau, Computation of ring statistics for network models of solids, Phys. Rev. B **44**, 4925 (1991).

[49] M. De Berg, M. Van Kreveld, M. Overmars, and O. Schwarzkopf, Computational geometry, in *Computational Geometry* (Springer, Berlin, 1997), pp. 1–17.

[50] See Supplemental Material at http://link.aps.org/supplemental/10.1103/PhysRevB.104.054208 for the process flow of RRD calculation.

[51] See Supplemental Material at http://link.aps.org/supplemental/10.1103/PhysRevB.104.054208 for PBG width vs RRD of an ordered gyroid under vertex relocation.

[52] H. Kang and Y. Zhu, Observation of Large Kerr Nonlinearity at Low Light Intensities, Phys. Rev. Lett. **91**, 093601 (2003).

[53] F. Evers and A. D. Mirlin, Fluctuations of the Inverse Participation Ratio at the Anderson Transition, Phys. Rev. Lett. **84**, 3690 (2000).

[54] J. M. Escalante and S. E. Skipetrov, Level spacing statistics for light in two-dimensional disordered photonic crystals, Sci. Rep. **8**, 11569 (2018).

[55] J. Ricouvier, P. Tabeling, and P. Yazhgur, Foam as a self-assembling amorphous photonic band gap material, Proc. Natl. Acad. Sci. USA **116**, 9202 (2019).

[56] See Supplemental Material at http://link.aps.org/supplemental/10.1103/PhysRevB.104.054208 for the evolution of PBG with respect to relocation distance for CRN′-RV.

Correction: The name of the first author was misspelled and has been fixed.